minerals

MDPI

Article

Integrated Membrane Process Coupled with Metal Sulfide Precipitation to Recover Zinc and Cyanide

Gabriel Seriche [1], Michelle Quilaqueo [1], Lorena Barros [1], Minghai Gim-Krumm [1], Ignacio Cortés [1,2], Elizabeth Troncoso [2,3], René Ruby-Figueroa [3] and Humberto Estay [1,*]

[1] Advanced Mining Technology Center (AMTC), University of Chile, Av. Tupper 2007 (AMTC Building), Santiago 8370451, Chile; gabriel.seriche@amtc.cl (G.S.); michelle.quilaqueo@amtc.cl (M.Q.); lorena.barros@amtc.cl (L.B.); minghai.gim@amtc.cl (M.G.-K.); ignacio.cortesm@utem.cl (I.C.)

[2] Department of Chemistry, Universidad Tecnológica Metropolitana, Las Palmeras 3360, Santiago 7800003, Chile; elizabeth.troncoso@utem.cl

[3] Programa Institucional de Fomento a la Investigación, Desarrollo e Innovación (PIDi), Universidad Tecnológica Metropolitana, Santiago 8940577, Chile; rruby@utem.cl

* Correspondence: humberto.estay@amtc.cl

Abstract: In gold cyanidation plants, which include a zinc cementation process, there is a progressive increase in zinc content in the solution and a higher cyanide concentration in leaching tailings. Consequently, there are opportunities to: (i) recover zinc and cyanide from these solutions, (ii) generate a saleable ZnS by-product, and (iii) reduce cyanide consumption and cyanide concentration in leaching tailings. Previous studies have proposed the use of the SART (Sulfidization, Acidification, Recycling, and Thickening) process for this purpose; however, this process has disadvantages that must be addressed. This study presents the results of the experimental assessment of an alternative process, the SuCy process, which uses an integrated membrane process. The SuCy process is composed of a metal sulfide precipitation coupled with a membrane filtration stage, a membrane contactor step to recover and concentrate cyanide, and a final neutralization and ultrafiltration stage. The flux obtained for zinc sulfide separation was around 0.01 L/m^{2}s, with cyanide recovery of 95% at 60 min, whereas flux for ultrafiltration was 0.22 L/m^{2}s. A comparison with an experimental study of the SART process at laboratory scale showed that the SuCy process could obtain a higher zinc recovery and can reduce the solid–liquid separation equipment by around five times. Therefore, the SuCy process could be a promising alternative for zinc and cyanide recovery in gold cyanidation.

Keywords: metal sulfide precipitation; membrane filtration; membrane contactors; SART process; SuCy process; gold cyanidation; zinc cementation; Merrill–Crowe; cyanide recovery; metal recovery

Citation: Seriche, G.; Quilaqueo, M.; Barros, L.; Gim-Krumm, M.; Cortés, I.; Troncoso, E.; Ruby-Figueroa, R.; Estay, H. Integrated Membrane Process Coupled with Metal Sulfide Precipitation to Recover Zinc and Cyanide. *Minerals* **2022**, *12*, 229. https://doi.org/10.3390/min12020229

Academic Editors: Longhua Xu and Benjamin P. Wilson

Received: 10 December 2021
Accepted: 7 February 2022
Published: 10 February 2022

1. Introduction

The conventional method to extract gold and/or silver from ores, tailings, or wastes is cyanidation. The recovery of gold from cyanide solutions can be conducted by zinc cementation, or the Merrill–Crowe (MC) process [1]. In gold plants with MC process, the zinc concentration increases progressively because the unique zinc output of the system is the leaching tailings, promoting a build-up of zinc in the cyanidation plant and the rise of cyanide concentration in solutions and leaching tailings. In this regard, there are studies proposing the use of the SART (Sulfidization, Acidification, Recycling and Thickening) process to recover zinc and cyanide, as an opportunity to produce a saleable by-product and to reduce cyanide consumption, respectively [2–5]. The SART process uses the metal sulfide precipitation method [6,7] in cyanide solution to remove copper (then recovery as a by-product) and regenerate free cyanide. Nevertheless, there are still no industrial experiences on recovering zinc and cyanide using the SART process, perhaps due to the low price of zinc, which limits the feasible economic window of this option [2], or due to the

characteristics of the zinc sulfide precipitate. ZnS precipitate presents colloidal behavior and low settling rates, affecting the solid–liquid separation stage [8]. In the latter, the option to assess different methods to perform the solid–liquid separation more efficiently could be needed to deal with these complex precipitates.

Recently, a membrane filtration process coupled with metal sulfide precipitation was proposed to recover copper from cyanide solutions [9] and from acid mine drainage (AMD) [10], obtaining permeate fluxes (i.e., separation rates) between 0.1 L/m²s and 1.4 L/m²s for different copper concentrations and operational conditions. These values and the compact design of membrane modules significantly reduce the residence time of the solid–liquid separation stage, from 90–120 min to less than 5 s, compared to a conventional thickener used in the SART process [11].

The membrane filtration coupled with metal sulfide precipitation is the first stage of this new integrated membrane process, proposed not only to recover copper, but to include a step for recovering a concentrated free cyanide solution and a final neutralization with ultrafiltration process to return an alkaline and treated solution to the cyanidation plant [11]. The SuCy process is proposed as an attractive alternative to the SART process due to its promising results. The SuCy process could enhance the process efficiency of copper and cyanide recovery with respect to the SART process, minimizing the plant size and the capital costs. The plant size reduction (up to 90%) can be very attractive for gold tailings reprocessing [12], when compact and mobile plants are advantageous in minimizing the transport of tailings.

The SuCy process (Figure 1) comprises three main stages: 1-Metal sulfide precipitation coupled with membrane filtration (microfiltration, MF) to recover a metal sulfide precipitate in a saleable form (ZnS for this case); 2-A gas-filled membrane absorption process (GFMA) [13] to transfer cyanide and concentrate it in an alkaline solution using membrane contactors [14]; 3-Neutralization with lime and gypsum separation through membrane ultrafiltration (UF).

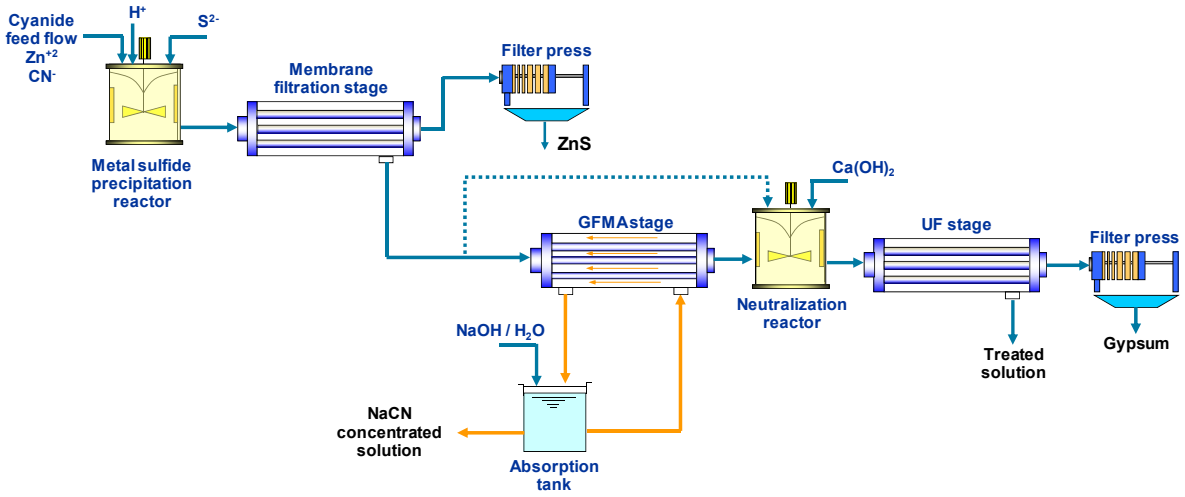

Figure 1. Schematic flow diagram of the SuCy process for zinc and cyanide recovery (Adapted with permission from reference [11], 2022, Elsevier).

To date, the SuCy process has been tested for cyanide solutions containing copper or copper and zinc only [11]. There is a lack of performance results for cyanide solutions having only zinc as the main metal, which can be expected in cyanidation plants with zinc cementation. This study presents the first assessment of the integrated membrane process (The SuCy process) at laboratory scale, targeting cyanide solutions containing zinc. In order to compare the results obtained from the SuCy process, experimental runs at lab-scale

were carried out using the SART process under the same operational conditions in order to establish comparisons in the process performance when using both alternatives.

2. Materials and Methods

2.1. Synthetic Cyanide Solution and Experimental Set-Up

A synthetic cyanide solution containing zinc was prepared using NaCN, $ZnSO_4 \cdot 7H_2O$ (reagent grade > 99%, Merck), and demineralized water (<5 µS/cm). Zinc and total cyanide concentration were fixed at 1500 mg/L and 2500 mg/L, respectively, to mimic real cyanide solutions with high zinc concentrations from gold plants with zinc cementation.

The MF and UF were conducted in the same prototype assembled, as shown in Figure 2, using different reagents, feed solution and membrane as required. This membrane filtration prototype included a jacketed, sealed, and stirred (200 rpm) 2 L reactor, where metal sulfide precipitation or neutralization was carried out. The reactor was temperature-controlled by a recirculated bath at 15°C. Reagent solutions used were NaHS 4 M solution, H_2SO_4 4 M solution, and $Ca(OH)_2$ suspension at 5.0% solids and 99% purity of lime.

A diaphragm pump fed the suspension into a monotubular membrane module (Valisette, Tami Industries, France) at 650 mL/min. The membrane module contained one ceramic membrane (TiO_2 with an active layer of TiO_2-ZrO_2) of 0.14 µm pore size in the case of MF, and 150 kDa of cut-off in the case of UF (Valisette, Tami Industries, Nyon, France), both with 0.005 m^2 filtration area. The trans-membrane pressure was controlled by a syringe valve located at the retentate flow. The MF and UF stages were conducted under batch-recirculation configuration, where the permeate is continuously removed, and the retentate is recycled into the reactor. A balance located under the permeate tank (2 L capacity) measured the permeate flow used to estimate the flux, according to the following equation:

$$J = \frac{V_p}{t \cdot A} \quad (1)$$

where J is the permeate flux (L/m^2s), V_P is the cumulated permeate volume (L) at a certain time t (s), and A is the membrane area (m^2).

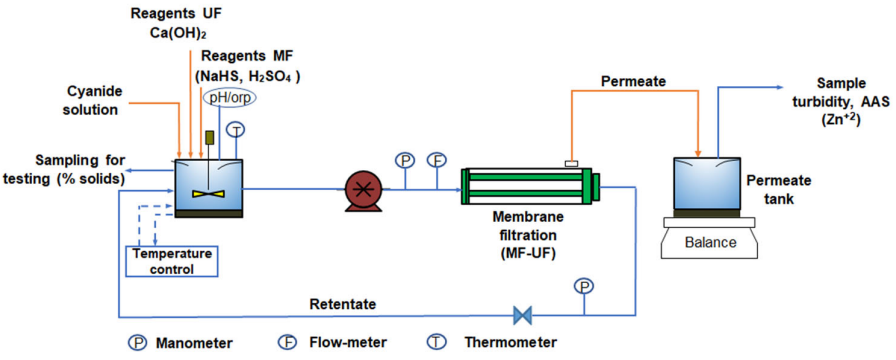

Figure 2. Simplified scheme of the MF and UF laboratory prototypes used for tests of metal sulfide precipitation and clarification, and neutralization and gypsum clarification, respectively. (Adapted with permission from reference [11], 2022, Elsevier).

For MF tests, samples were collected from the reactor tank at the beginning and the end of each test by a syringe filter (0.2 µm pore size). Both samples were neutralized with NaOH 1 M solution to obtain a pH 12, and they were analyzed by AAS (AAS, GBC Scientific Equioment, model SensAA dual, Braeside, Austalia) for zinc. The zinc conversion was estimated according to the following equation.

$$\text{Conv.} = \frac{\text{Zn}_0 - \text{Zn}_f}{\text{Zn}_0} 100 \quad (2)$$

where Conv. is the zinc conversion (%), Zn_0 is the initial zinc mass contained in the cyanide solution (mg), and Zn_f is the final zinc mass in the reactor tank or the permeate tank (mg). The conversion estimated in the permeate tank represents the overall conversion of the SuCy process. The cyanide concentration in the permeate tank was measured by $AgNO_3$ 1 M titration with potentiometric end-point in an automatic titrator (Methrom, Model 888 Titrando, Herisau, Switzerland). A final sample taken from the suspension remaining in the reactor was filtered, washed and then dried to be analyzed by X-ray fluorescence (XRF) in order to determine the elemental characterization of solid precipitates. Precipitates collected from the MF stage were a whole composite of the final suspension.

The permeate solution generated by the MF stage was fed into a 2 L sealed, jacketed, and stirred feed tank of the GFMA stage (Figure 3). The pH was adjusted at 4.5 with H_2SO_4 1 M solution, and then the solution was fed into a hollow fiber membrane contactor (HFMC) module (MiniModule 1.7 × 5.5, 3 M LiquiCel™, Charlotte, NC, USA) by the shell side, whereas the absorption solution (NaOH solution at 5 wt. %) was fed into the HFMC module by the lumen side from the 2 L sealed, jacketed, and stirred absorption tank. Samples were collected from the feed and absorption tanks to measure the cyanide concentration by $AgNO_3$ 1 M titration with potentiometric end-point at different times. Cyanide recovery at each time was estimated according to the following equation:

$$\text{RecCN}_t = \frac{\text{CN}_0 - \text{CN}_t}{\text{CN}_0} 100 \quad (3)$$

where $RecCN_t$ is the cyanide recovery (%) at a certain time t (min), CN_0 is the mass of cyanide (mg) at time 0 min in the feed solution, and CN_t is the mass of cyanide (mg) at time t in the feed tank.

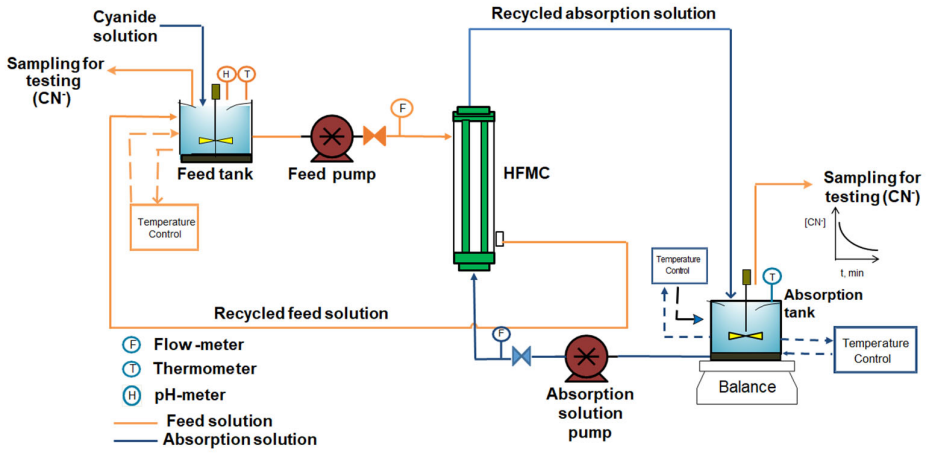

Figure 3. Schematic representation of the GFMA prototype at laboratory scale for tests of HCN recovery in the form of NaCN. (Adapted with permission from reference [11], 2022, Elsevier).

The neutralization was performed until reaching a pH value of 10.5 by lime. The suspension generated in the reactor was fed into the membrane module at 2 bar of transmembrane pressure (TMP). At the end of the test, the permeate turbidity was measured by a turbid-meter (Hanna Instruments, HI 88703-02, Santiago, Chile).

The methodology and experimental set-up for the membrane separation systems were identical to our previous study [11]. All tests were conducted at pH 3.5 and with sulfide stoichiometric dosage of 120% with respect to zinc. In this case, the residence time in the reactor was 15 min and the TMP for MF of zinc sulfides was determined here.

2.2. Characterization of Zinc Sulfide Precipitates

A sulfide precipitation test at pH 3.5 and 120% NaHS stoichiometric dosage was performed in the reactor at 15°C with the aim of obtaining zinc sulfide precipitates. The resulting sample was analyzed using optical microscopy (Leica, model DM 750, connected to a digital camera HD 5 MGPXL WI-FI, Leica ICC50W, Wetzlar, Germany) to determine the aggregation behavior. Particle size distributions were also determined using laser diffraction (Malvern Mastersizer 2000, Malvern Panalytical Ltd., Malvern, UK).

2.3. Determination of Limiting Flux and Critical TMP

Limiting flux (J_L) and critical TMP (TMP_C) were determined using the MF prototype (Figure 2), following the same methodology described in Section 2.1. Different tests were carried out for TMP, ranging between 1 and 3 bar. A curve between average flux and TMP allowed determining the TMP_C and J_L [15].

2.4. Sequential Tests of the SuCy Process

Sequential tests for the SuCy process were conducted according to the methodology described in our previous study [11] and using the synthetic solution defined in 2.1 (solution at pH 3.5 and 120% sulfide stoichiometric dosage). The TMP of the MF stage was fixed at 1.0 bar, according to the TMP_C results (see Section 3.2).

During these tests, the cyanide synthetic solution was sequentially treated in each stage of the SuCy process under batch conditions. This meant that the generated permeate in the MF stage was then processed in the GMFA process. After that, the resulting solution from the GFMA step was treated in the neutralization and UF stage.

Additionally, the fouling mechanism in the MF test was analyzed using the Hermia model [16] modified for cross-flow [15], which comprised four equations derived from the value of n of the general equation:

$$\frac{d^2t}{dt} = K(J - J_{ss})J^{2-n} \quad (4)$$

where *n* is the type of fouling (n = 2 is the complete pore blocking, *n* = 1.5 is the Standard pore blocking, n = 1 is the Intermediate pore blocking, and *n* = 0 is the Cake formation), J_{ss} can be taken as the "steady-state flux" achieved at long times, and K is a constant depending on the fouling phenomena. The adjustment of the experimental data to the fouling model was performed by a least-squares fitting procedure [10,17]. In addition, validation of each model was performed using the residual analysis to corroborate that these residuals come from a normal distribution. This process ensures that none of the explanatory or predictive information of the model is included in the error. In this sense, Shapiro–Wilk and Kolmogorov–Smirnov statistics were used for this purpose. The statistic and mathematical computations were performed in Statgraphics Centurion 19 (Statgraphics Technologies, VA, USA).

2.5. Tests of the SART Process

A test of the SART process was also performed using the same prototype and experimental methodology described in our previous study for copper recovery [11]. The SART prototype (Figure 4) comprised a feed tank (25 L) of cyanide solution containing zinc (identical to the solution tested for the sequential SuCy process), a sealed and stirred precipitation reactor (1 L), a gravitational clarifier of 15 cm diameter and 60 cm length, and a stirred neutralization reactor (2 L). This small-scale prototype was operated under steady-state conditions. NaHS 1 M and H_2SO_4 1 M solutions were added into the precipitation reactor by two dosage pumps to keep pH 3.5 and 120% sulfide stoichiometric addition. The feed flow of cyanide solution was around 90 mL/min. Flocculant (FL2030, supplied by SNF) solution 0.5 g/L was fed into the feed-pipe of the clarifier. A fraction of the underflow (80%) was semi-continuously recycled into the reactor in order to keep a constant

bed volume at the system and then analyzed by XRF (therefore, suspended solids were not analyzed). Finally, the clarifier overflow was neutralized with lime suspension to reach a pH value of 10.5. The overflow discharged from the neutralization tank was finally collected in a reception tank.

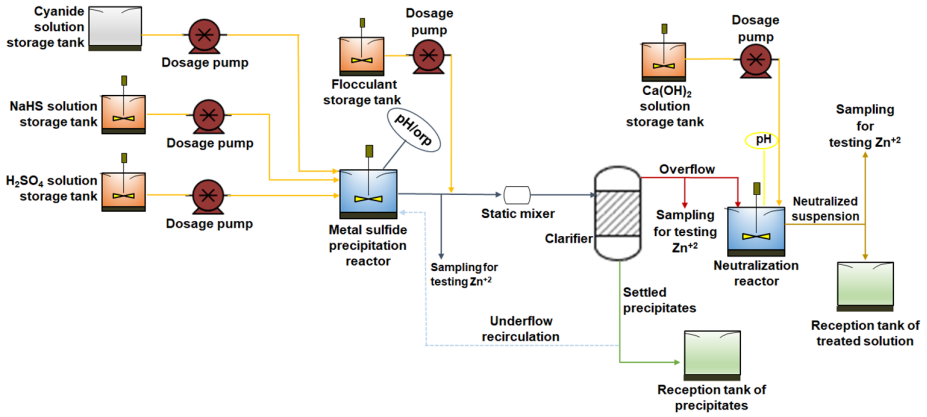

Figure 4. Schematic representation of SART small-scale prototype. (Adapted with permission from reference [11], 2022, Elsevier).

Samples were collected in the overflow of the precipitation reactor, the overflow of the clarifier, and the overflow of the neutralization reactor to be analyzed by AAS for zinc. A sample from the clarifier overflow without filtering was analyzed in a turbid-meter.

3. Results

3.1. Characterization of the Zinc Sulfide Precipitates

Optical microscopy and laser diffraction techniques were used to determine the aggregation behavior and particle size distribution of precipitates as shown in Figure 5. The precipitates generated tended to form small clusters of aggregates, with a maximum size of ~ 50 μm. This result agreed with visual observations, as can be seen in the micrograph in Figure 5. These aggregates were smaller than those obtained for copper sulfide precipitates, which reached sizes even above 500 μm [11]. The particle size distribution (PSD) shows that 91% of particles were smaller than 10 μm, and 17% were even below 1 μm. These values confirm that zinc sulfide precipitates are fine and small. Likewise, these results are in line with previous studies [8,18,19]. The fraction smaller than 0.5 μm (~3%) establishes that the pore size of the membrane chosen for the first stage must be smaller than 0.2 μm. Therefore, this result confirms the correct pore size selection (0.14 μm) for the membrane used in the MF stage.

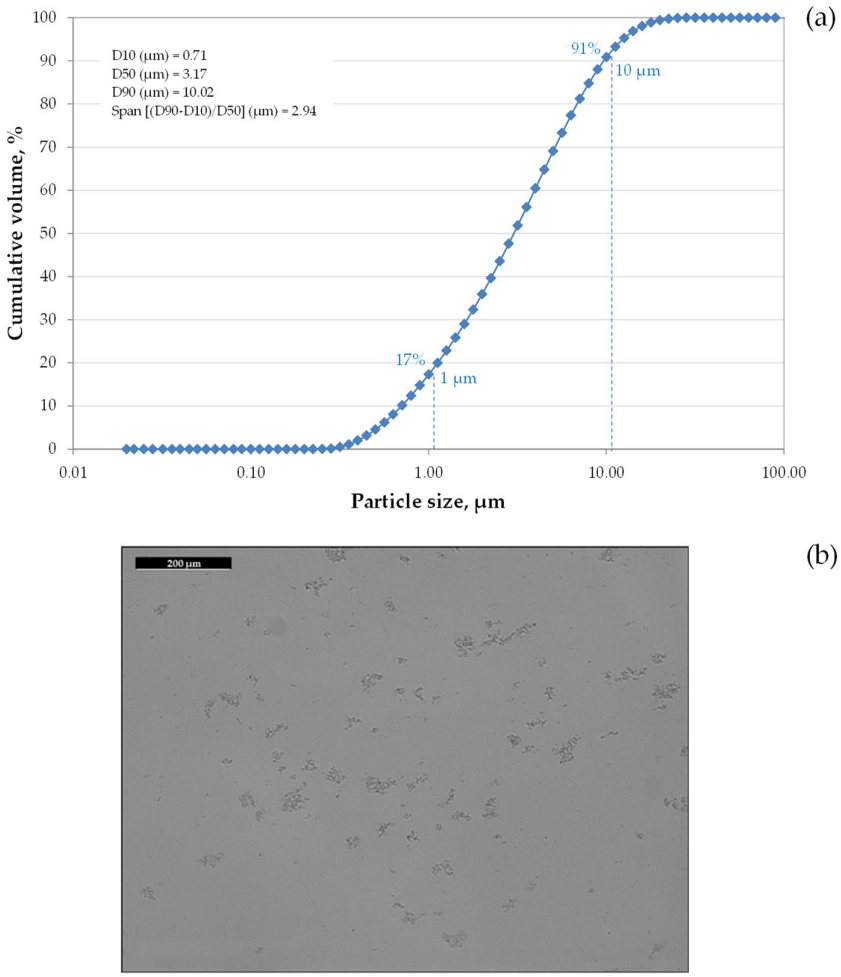

Figure 5. Characterization results of the zinc sulfide precipitates. (**a**) Particle size distribution obtained by a laser diffraction method, and (**b**) micrograph obtained by optical microscopy.

In addition, particle size distributions can be characterized in terms of the span, which gives an indication of the distance between the 10th (D10) and 90th (D90) percentile, normalized with respect to the 50th percentile (D50) [A,B]. A smaller span indicates a narrower particle size distribution [20]; however, the span obtained here was 2.94 (span>1), which indicates that size distribution can be considered as non-homogeneous.

3.2. Determination of TMP$_C$ and J$_L$

Results of flux at different TMP levels are shown in Figure 6. This curve confirms a TMP$_C$ value of 2.0 bar. Therefore, the J$_L$ is around 0.023 L/m^{2}s. According to these results, the operational TMP should be between 0.5 and 1.5 bar in order to avoid the operation near the J$_L$ [15,21].

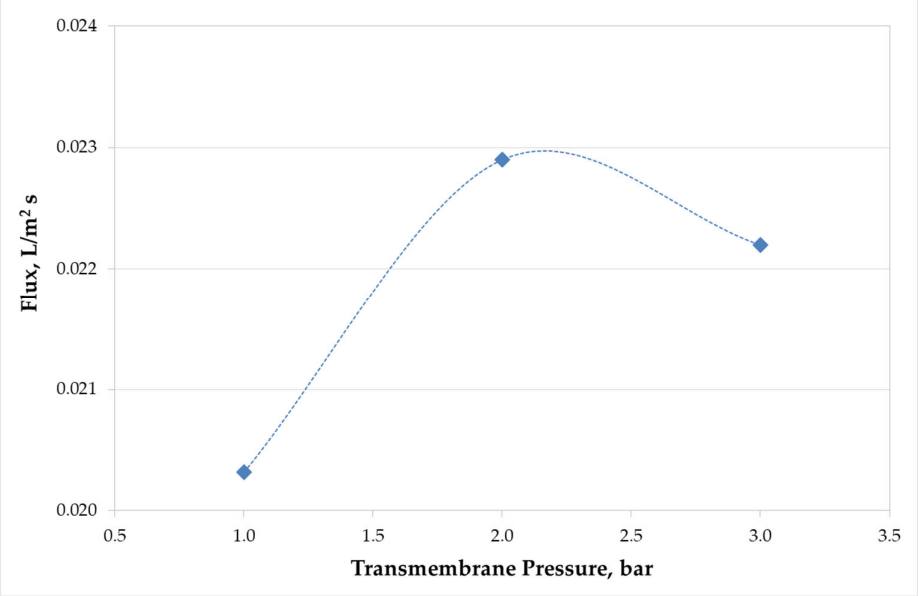

Figure 6. Variation of permeate flux with respect to TMP for zinc sulfide precipitates at pH 3.5 and 120% sulfide stoichiometric dosage.

The operational TMP selected for this study was 1.0 bar, different from the TMP selected for copper precipitates, which was 2.0 bar [9]. Thus, the operational feed pressure will be lower than the TMP_C, and keeping the same point measured here, but at industrial scale, the feed pressure could range between 0.5 and 1.5 bar. The aggregation behavior of zinc precipitates, which tend to form bonds with water, drastically opposes copper sulfide precipitates, since they are more hydrophobic and thus prefer bonding with other copper precipitates instead of water [8,18]. Therefore, the fouling generated by zinc precipitates is more detrimental than copper precipitates in flow resistance.

3.3. Sequential Tests of the SuCy Process

The permeate flux curve for the MF stage is shown in Figure 7, where a progressive decline is observed until reaching values of 0.01 L/m²s at the end of the test. This flux value is two orders of magnitude lower than those maximum values obtained for copper sulfide precipitates [11]. In addition, the tendency towards a continuous decline in the flux curve for this case differs from the flux curve observed for copper precipitates in cyanide solutions, where the tendency did not show a decline during the test [9,11]. The aggregates characteristics and small size of zinc sulfide can explain this significant difference between both metal sulfide precipitates. In fact, the tendency of the flux curve of this case is similar to the real solution tested in our previous study [11], which contained around 300 mg/L zinc, but the Cu/Zn molar ratio was 1.9. Hence, zinc precipitates promote a detrimental performance when copper precipitates are present. Future studies could be focused on determining a critical Cu/Zn molar ratio where flux declines significantly.

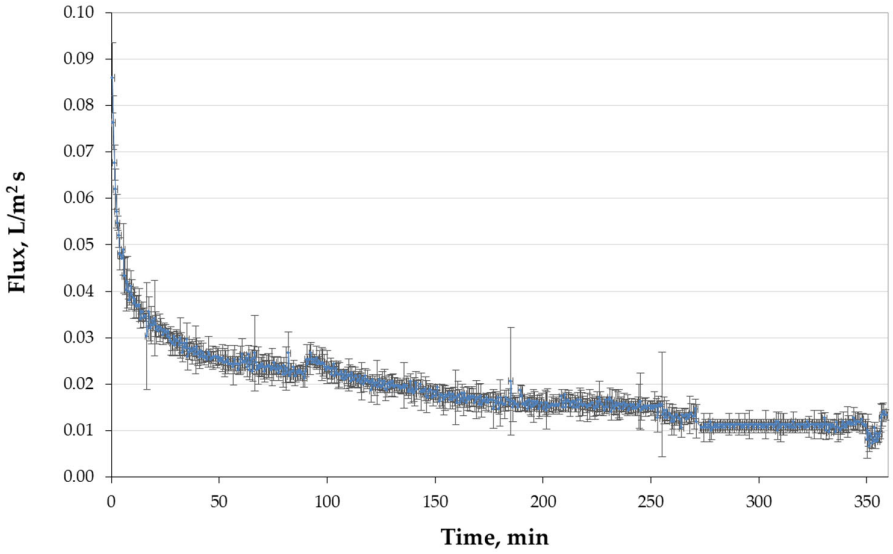

Figure 7. Variation of permeate flux with respect to time in the MF stage for zinc sulfide precipitates at pH 3.5 and 120% sulfide stoichiometric dosage.

The analysis of membrane fouling (Table 1) translates into the correlation of permeate flux data with different types of fouling mechanism affecting the membrane, showing that none of the models has been statistically validated given the normal distribution in its residuals. Despite that, the models that showed higher values of R^2 and lower values of RSME (Table 1) were those related to cake formation, followed by standard blocking and intermediate blocking, with R^2 (coefficient of determination) values of 92.5, 87.2 and 86.2%, respectively. The above indicates that, in the MF experiment, different mechanisms could have been acting simultaneously. During the experiment, some particles that did not enter the pores formed a cake layer on the membrane surface, a process known as cake formation. Alternatively, some particles smaller than the pores entered the membrane pore, reducing the pore volume, a process known as standard blocking. In contrast, other particles obstructed the pore entrance, but did not block it completely, producing the so-called intermediate blocking. These mechanisms have a direct relation to the tendency of the permeate flux obtained (Figure 7), where a progresive decline can be observed.

Table 1. Fitted parameters for fouling models according to the modified Hermia models for cross-flow filtration, unified model of flux decline, and statistical model analysis for the studied membranes. S-W: Shapiro–Wilks test; K-S: Kolmogorov–Smirnov test; RMSE: root mean square error.

Type of Fouling	Equation	Fitted Model Parameters and Statistical Model Analysis	Values
Complete blocking	$J = (J_o - J_{ss})exp\,(-K_c t) + J_{ss}$	Kc	8.45×10^{-4}
		R^2 (%)	65.50
		RSME	1.71×10^{-10}
		S-W test (p-value)	≤0.05
		K-S test (p-value)	≤0.05
Standard blocking	$J = (J_o^{-0.5} + K_s t)^{-2}$	Ks	2.17×10^{-2}
		R^2 (%)	87.20
		RSME	1.06×10^{-10}
		S-W test (p-value)	≤0.05
		K-S test (p-value)	≤0.05

Intermediate blocking	$J = \frac{J_{ss}}{\left[1 - \left(\frac{J_o - J_{ss}}{J_o}\right) exp\ (-J_{ss} K_i t)\right]}$	Ki	14.75
		R^2 (%)	86.20
		RSME	2.18×10^{-11}
		S-W test (p-value)	≤0.05
		K-S test (p-value)	≤0.05
Cake formation	$K_g t = \frac{1}{J_{ss}^2}\left[ln\left(\frac{J}{J_o} * \frac{J_o - J_{ss}}{J - J_{ss}}\right) - J_{ss} * \left(\frac{1}{J} - \frac{1}{J_o}\right)\right]$	Kg	445,538
		R^2 (%)	92.50
		RSME	1.25×10^{-11}
		S-W test (p-value)	≤0.05
		K-S test (p-value)	≤0.05

Results for the cyanide recovery in the GFMA process are shown in Figure 8. It can be seen that this recovery reached a value of 95% at 60 min. These results agreed with previous values obtained for sequential tests of copper precipitates [11] and for cyanide solutions in similar conditions [22].

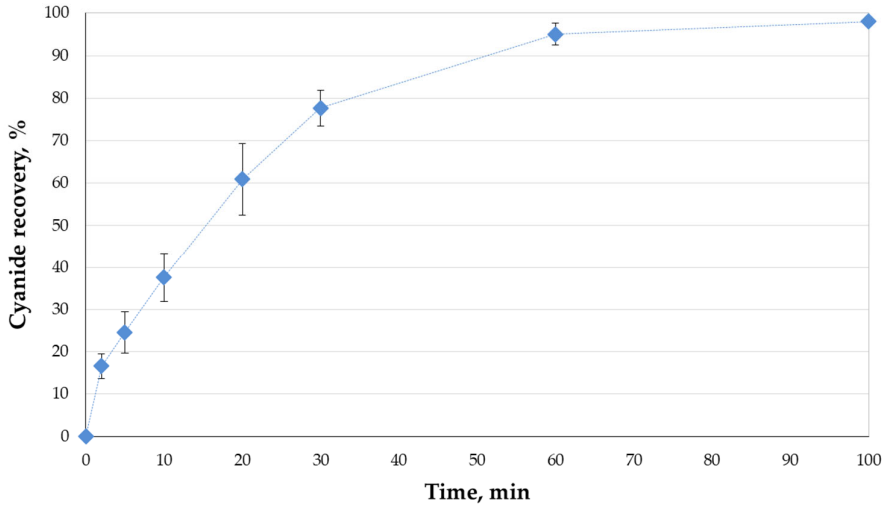

Figure 8. Cyanide recovery vs. time in the GFMA process after treating the permeate obtained in the MF stage.

The solution with low contents of cyanide and zinc was processed in a neutralization stage. The suspension formed here was fed into a UF membrane stage. Flux results of gypsum separation are shown in Figure 9. The flux curve presented a slight decline tending to a plateau of 0.22 L/m²s. This value was slightly lower than that obtained for the sequential tests for copper precipitates of around 0.25–0.3 L/m²s.

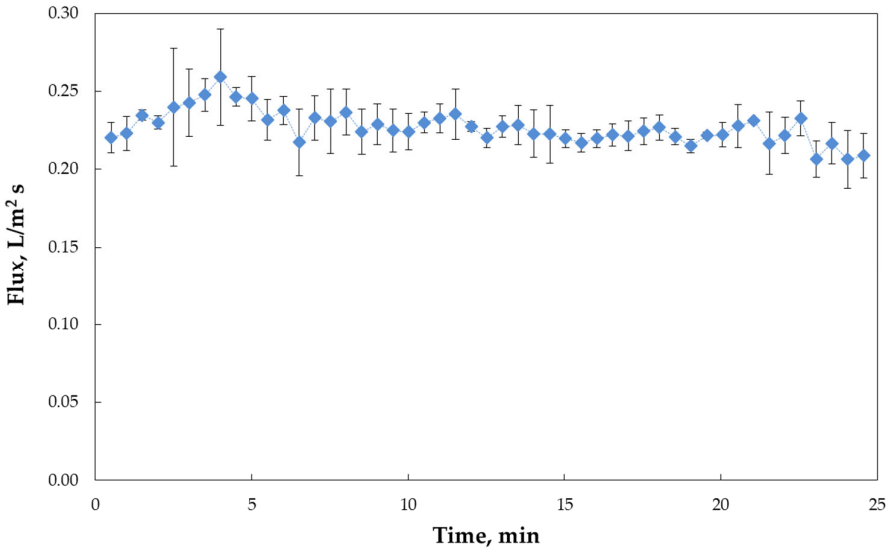

Figure 9. Variation of permeate flux with time, obtained in the UF stage for gypsum formed after neutralization at pH 10.5.

A summary with additional results is shown in Table 2. Zinc recovery was maximum for the permeate of the MF stage, demonstrating that the SuCy process can efficiently recover and separate metal sulfide precipitates. The zinc content in the precipitates was closer to the stoichiometric value of ZnS. Differences could be attributed to traces of sulfate crystallized salts remaining after the washing and filtering processes. On the other hand, the final concentration of titratable cyanide in the MF stage was lower than the initial total cyanide solution prepared. Taking into account the zinc recovery, the cyanide concentration associated with zinc should be disregarded, and therefore the titratable cyanide measured should be similar to free cyanide. According to these results, almost 10% of the cyanide was lost in the MF stage, probably due to HCN volatilization in the reactor, SCN^- generation or cyanide oxidation. The HCN flux of the GFMA process was similar to the case study of copper precipitate. Finally, the permeate turbidity in the UF was lower than 0.5 NTU, demonstrating the efficient separation of gypsum.

Table 2. Additional results of sequential tests for the SuCy process.

Parameter	Value
Zn recovery in reactor, %	97.8
Overall Zn recovery, %	~100
Solids content in retentate of MF, %	3.7
Zn content in precipitate, %	66.6
S content in precipitate, %	31.2
Titratable cyanide concentration at the end of MF stage, mg/L	2270
Free cyanide concentration in the solution treated at the end of GFMA process, mg/L	36.5
HCN flux in GFMA at 60 min, mg/m²s	2.2
Permeate turbidity in UF, NTU	0.3

3.4. Test of the SART Process

Zn conversion in the SART prototype was measured in the sulfide precipitation reactor (discharge), in the thickener overflow, and in the neutralization reactor. Figure 10 shows the Zn conversion in each point of the system according to time. The average Zn conversion was 94.5%, 93.6%, and 96.0% in the sulfide precipitation reactor, in the thickener overflow, and in the neutralization reactor, respectively. Even though the conversion tended to increase after 200 min of operation, the Zn conversion in the final flow of the

process (neutralization reactor) was lower, between 1% and 2%, than the one compared to the sulfide precipitation reactor. In this case, the separation efficiency of the thickening stage plays a relevant role. Figure 11 shows the turbidity evolution in the thickener overflow, where the values obtained ranged between 120 NTU and 190 NTU. The zinc precipitates in the overflow explain the decrease in zinc conversion. Figure 12 shows pictures of the lab-scale thickener used, where the interphase of settled solids and the clarified solution can be observed. The clarified solution was white because of the presence of fine ZnS precipitates, and despite of the use of flocculant and the high residence time of the equipment (~3 h). The fine ZnS particles were lost in the overflow, reducing the zinc conversion. The high residence time of thickener also could explain the decline in zinc conversion in the thickener overflow and in the neutralization reactor between 150 and 200 min. There is a retarded response to the zinc recovery obtained in the precipitation reactor before 50 min.

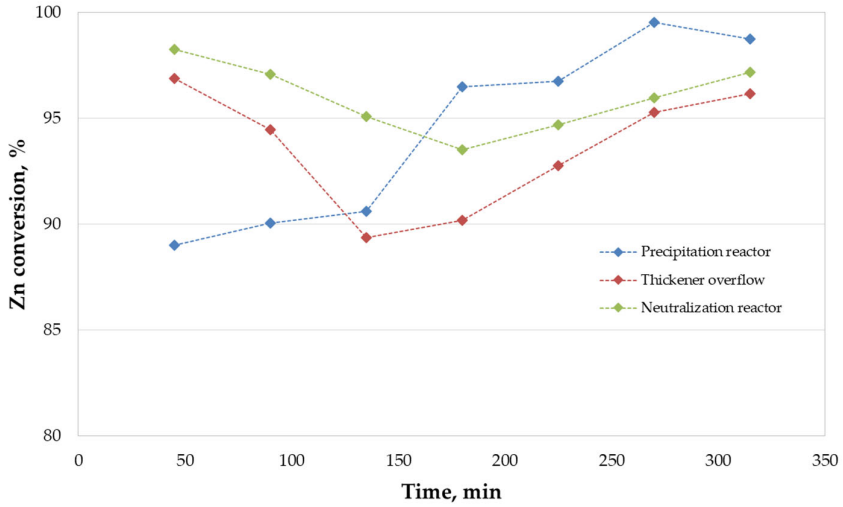

Figure 10. Zn conversion in the SART process vs. time in each stage of the plant.

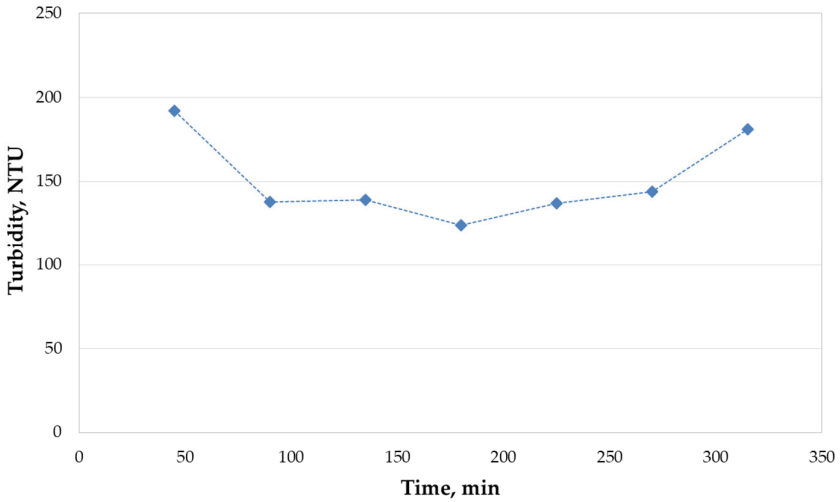

Figure 11. Thickener overflow turbidity vs. time in the SART process.

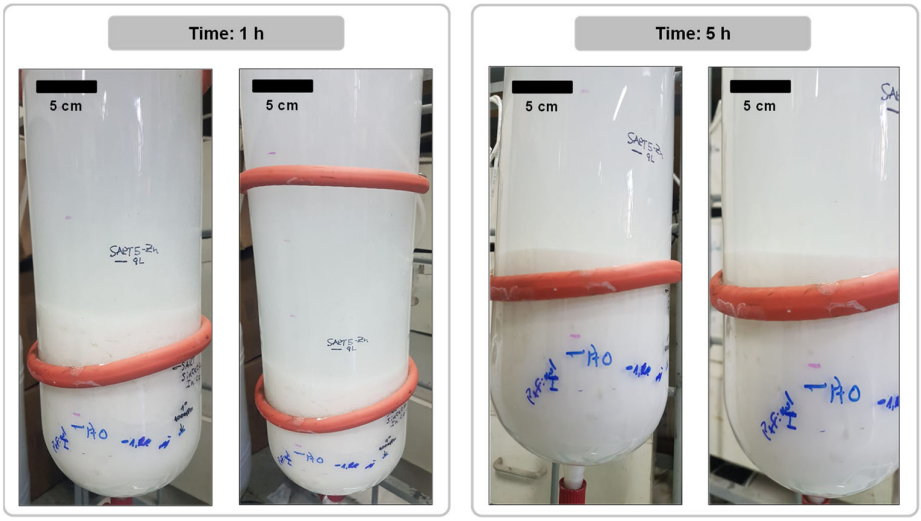

Figure 12. Pictures of lab-scale thickener in the SART process.

Table 3 shows additional results obtained in the SART process tests. Solid content obtained in the thickener underflow was similar to that obtained in the retentate of the SuCy process (see Table 2). Moreover, zinc and sulfur contents in the precipitate were also similar to those obtained from the SuCy process, although the zinc grade was slightly higher, even exceeding the stoichiometric value of ZnS. This fact could be explained given the adsorption of dissolved zinc as zinc–cyanide complex or zinc sulfate on precipitates surface.

Table 3. Additional results of the SART process.

Parameter	Value
Solids content in thickener underflow, %	3.7 ± 0.8
Zn content in precipitate, %	69.7
S content in precipitate, %	28.6

4. Discussion

In this study, the application of the SuCy process for recovering zinc and cyanide showed interesting results, similar to those obtained previously for copper and cyanide recovery in the GFMA and UF unit operations. However, permeate flux values of MF applied to zinc sulfide precipitates (see Figure 7) were two orders of magnitude lower than those obtained for copper sulfide precipitates [11]. This difference can be explained by the aggregation behavior of the zinc sulfide precipitates, which have hydrophilic characteristics, contrary to copper sulfide precipitates, which present a hydrophobic behavior [8,18]. Therefore, the particle size of zinc sulfide precipitates is lower than copper sulfide precipitates. This results in a more detrimental fouling formation in the MF membrane.

In comparison to the SART process, the SuCy process could enhance the overall zinc recovery, producing a concentrated cyanide solution and producing a clear final permeate, obtaining a similar product of zinc sulfide in terms of zinc content and solids concentration in the final suspension. Although the flux value for zinc sulfide clarification was lower than the clarification of copper, the compact design of membrane modules allowed obtaining smaller equipment volume than the SART process. For instance, the treatment of 200 m^3/h of feed cyanide solution with 1500 mg/L Zn in an MF stage with 0.01 L/m^2s of MF flux implies that the total area required is 5556 m^2. The larger industrial ceramic membrane modules have around 110 m^2, with 1.2 m of length and 1.2 m of diameter, defining 51 membrane modules and a total equipment volume of 69 m^3. In the case of the SART process, the thickening stage typically uses a rise rate of 2.0 m^3/m^2h, showing a thickener

diameter of 11.3 m with a volume of approximately 250 m^3, i.e., 3.6 times higher than the MF clarification stage of the SuCy process. Even though this difference is lower than in the case of copper precipitates separation, the SuCy process is thus an attractive alternative to the SART process. However, further economic assessments should be explored to compare both options.

Finally, future research should be conducted to assess behavior under different operational conditions, for example, varying the pH and sulfide stoichiometric dosage. Although previous studies have shown that the increase in pH promotes a decline in zeta potential [8,23], which indicates that precipitates tend to disaggregate, they might be detrimental for solid–liquid separation performance. In this context, additional studies, including investigating different ways to increase the aggregation capacity of zinc sulfide precipitates, could allow the optimization of the SuCy process for zinc recovery.

5. Conclusions

The SuCy process has been tested at laboratory scale for recovering zinc sulfide precipitates and a concentrated cyanide solution. Results showed low flux values after the separation of zinc sulfide precipitates in the MF stage, reaching around 0.01 L/m^2s. This value was approximately two orders of magnitude lower than those obtained in previous studies for copper sulfide precipitates clarification in MF. This significant difference is explained by the aggregation behavior found for zinc sulfide and copper sulfide precipitates. On the one hand, whilst copper precipitates tend to form large aggregates due to the hydrophobic characteristics of copper sulfide, instead zinc sulfide forms smaller aggregates because of its hydrophilic characteristics. On the other hand, the GFMA and neutralization stages with UF presented similar results to previous studies for copper recovery, reaching 95% of cyanide recovery at 60 min and flux in UF of 0.22 L/m^2s. In comparison to the SART process, the SuCy process obtains high zinc recoveries, even considering its low flux for zinc sulfide. A preliminary equipment sizing demonstrated that this process could reduce the separation for the solid–liquid separation stage by five times. Therefore, the SuCy process could be an interesting alternative for recovering zinc and cyanide in gold cyanidation plants with high zinc contents in their solutions.

6. Patents

A SuCy process patent was presented in January 2020 at the Chilean patent office (INAPI). The patent number is INAPI PCT/CL2020/050005.

Author Contributions: Conceptualization, H.E. and R.R.-F.; methodology, G.S, M.Q, L.B, M.G-K., and I.C.; validation, G.S., L.B., and M.Q.; formal analysis, H.E., R.R.-F., and E.T.; investigation, G.S. and L.B.; resources, H.E.; data curation, H.E. and E.T.; writing—original draft preparation, H.E., R.R.-F., and E.T.; writing—review and editing, H.E., R.R.-F., and E.T.; visualization, E.T.; supervision, H.E.; project administration, H.E.; funding acquisition, H.E. All authors have read and agreed to the published version of the manuscript.

Funding: This research was funded by the National Commission for Scientific and Technological Research (CONICYT Chile) through the CONICYT-PIA Project AFB180004, CONICYT+FONDEF/CONCURSO IDeA I + D, FONDEF/CONICYT 2017 + ID17I10021 and FONDEF/CONICYT 2017 + ID17I20021 and The APC was funded by MDPI, H.E., R.R-F., and E.T.

Data Availability Statement: The data presented in this study are available within the manuscript.

Conflicts of Interest: The authors declare no conflict of interest. The funders had no role in the design of the study; in the collection, analyses, or interpretation of data; in the writing of the manuscript, or in the decision to publish the results.

References

1. Walton, R. Zinc cementation. In *Gold Ore Processing: Project Development and Operations*, 2nd ed.; Adams, M.D., Ed.; Elsevier: Amsterdam, The Netherlands, 2016; pp. 553–560. https://doi.org/10.1016/S0167-4528(05)15024-8.
2. Estay, H. Designing the SART process—A review. *Hydrometallurgy* **2018**, *176*, 147–165. https://doi.org/10.1016/j.hydromet.2018.01.011.
3. Estay, H.; Gim-Krumm, M.; Quilaqueo, M. Two-stage SART process: A feasible alternative for gold cyanidation plants with high zinc and copper contents. *Minerals* **2018**, *8*, 392. https://doi.org/10.3390/min8090392.
4. Littlejohn, P.; Kratochvil, D.; Hall, A. Sulfidisation-acidification-recycling-thickening (SART) for complex gold ores. In Proceedings of the World Gold 2013 Conference, Brisbane, Australia, 26–29 September 2013; pp. 149–155.
5. Sanguinetti, D.; Mohammadi, F.; Lopez, O. SART to remove zinc and copper from a silver Merrill Crowe barren leach solution. In Proceedings of the HydroProcess 2014, 6th International Workshop on Process Hydrometallurgy, Viña del Mar, Chile, 23–25 July 2014.
6. Lewis, A.E. Review of metal sulphide precipitation. *Hydrometallurgy* **2010**, *104*, 222–234. https://doi.org/10.1016/j.hydromet.2010.06.010.
7. Estay, H.; Barros, L.; Troncoso, E. Metal sulfide precipitation: Recent breakthroughs and future outlooks. *Minerals* **2021**, *11*, 1385. https://doi.org/10.3390/min11121385.
8. Gim-Krumm, M.; Quilaqueo, M.; Rojas, V.; Seriche, G.; Ruby-Figueroa, R.; Cortés-Arriagada, D.; Romero, J.; Troncoso, E.; Estay, H. Impact of precipitate characteristics and precipitation conditions on the settling performance of a sulfide precipitation process: An exhaustive characterization of the aggregation behavior. *Hydrometallurgy* **2019**, *189*, 105150. https://doi.org/10.1016/j.hydromet.2019.105150.
9. Estay, H.; Ruby-Figueroa, R.; Gim-Krumm, M.; Seriche, G.; Quilaqueo, M.; Díaz-Quezada, S.; Cortés, I.; Barros, L. Changing the conventional clarification method in metal sulfide precipitation by a membrane-based filtration process. *J. Mater. Sci. Technol.* **2021**, *11*, 693–709. https://doi.org/10.1016/j.jmrt.2021.01.034.
10. Menzel, K.; Barros, L.; García, A.; Ruby-Figueroa, R.; Estay, H. Metal sulfide precipitation coupled with membrane filtration process for recovering copper from acid mine drainage. *Sep. Purif. Technol.* **2021**, *270*, 118721. https://doi.org/10.1016/j.seppur.2021.118721.
11. Estay, H.; Ruby-Figueroa, R.; Quilaqueo, M.; Seriche, G.; Cortés, I.; Gim-Krumm, M.; Barros, L. Enhancing the effectiveness of copper and cyanide recovery in gold cyanidation: A new integrated membrane process. *Hydrometallurgy* **2021**, *202*, 105606. https://doi.org/10.1016/j.hydromet.2021.105606.
12. Medina, D.; Anderson, C.G. A review of the cyanidation treatment of copper-gold ores and concentrates. *Metals* **2020**, *10*, 897. https://doi.org/10.3390/met10070897.
13. Estay, H.; Troncoso, E.; Ruby-Figueroa, R.; Romero, J. Performance evaluation of mass transfer correlations in the GFMA process: A review with perspectives to the design. *J. Membr. Sci.* **2018**, *554*, 140–155. https://doi.org/10.1016/j.memsci.2018.02.064.
14. Drioli, E.; Criscuoli, A.; Curcio, E. *Membrane Contactors: Fundamentals, Applications and Potentialities*; Elsevier: Amsterdam, The Netherlands, 2011.
15. Field, R.W.; Wu, D.; Howell, J.A.; Gupta, B.B. Critical flux concept for microfiltration fouling. *J. Memb. Sci.* **1995**, *100*, 259–272. https://doi.org/10.1016/0376-7388(94)00265-Z.
16. Hermia, J. Constant pressure blocking filtration laws-application to power-law non-newtonian fluids. *Trans. Inst. Chem. Eng.* **1982**, *60*, 183–187.
17. Mora, F.; Pérez, K.; Quezada, C.; Herrera, C.; Cassano, C.; Ruby-Figueroa, R. Impact of membrane pore size on the clarification performance of grape marc extract by microfiltration. *Membranes* **2019**, *9*, 146. https://doi.org/10.3390/membranes9110146.
18. Xia, Z.; Peng, X.; Kong, L.; Hu, X. Hydrophilicity/hydrophobicity of metal sulfide particles as a determinator of aggregation performance in wastewater. *J. Water Process Eng.* **2021**, *40*, 101900. https://doi.org/10.1016/j.jwpe.2020.101900.
19. Fleming, C.A.; Melashvili, M. The SART process: Killing the sacred cows. In Proceedings of the XXVIII International Mineral Processing Congress (IMPC 2016), Quebec City, QC, Canada, 11–15 September 2016.
20. Miller, J.; Mulligan, P.; Johnson, C.E. Comminution of pulverized Pittsburgh coal during ASTM E1226-12a dust combustibility testing. *Powder Technol.* **2020**, *375*, 28–32. https://doi.org/10.1016/j.powtec.2020.07.059.
21. Astudillo-Castro, C.L. Limiting flux and critical transmembrane pressure determination using an exponential model: The effect of concentration factor, temperature, and cross-flow velocity during casein micelle concentration by microfiltration. *Ind. Eng. Chem. Res.* **2015**, *54*, 414–425. https://doi.org/10.1021/ie5033292.
22. Quilaqueo, M.; Seriche, G.; Valetto, S.; Barros, L.; Díaz-Quezada, S.; Ruby-Figueroa, R.; Troncoso, E.; Estay, H. An experimental study of membrane contactor modules for recovering cyanide through a gas membrane process. *Membranes* **2020**, *10*, 105. https://doi.org/10.3390/membranes10050105.
23. Mokone, T.P.; van Hille, R.P.; Lewis, A.E. Effect of solution chemistry on particle characteristics during metal sulfide precipitation. *J. Colloid. Interface Sci.* **2010**, *351*, 10–18. https://doi.org/10.1016/j.jcis.2010.06.027.